




Dual gatekeepers-modified dendritic mesoporous silica nanoparticles for controlled drug release

Sheng-Nan Zhao¹, Run-Hua Tang¹, Shu-Jun Deng¹, Gui-E Chen^{1,*} , Jing Ye^{1,*}, and Zhen-Liang Xu^{2,*}

¹ School of Chemical and Environmental Engineering, Shanghai Institute of Technology, 100 Haiquan Road, Shanghai 201418, China

² State Key Laboratory of Chemical Engineering, Membrane Science and Engineering R&D Lab, Chemical Engineering Research Center, School of Chemical Engineering, East China University of Science and Technology, 130 Meilong Road, Shanghai 200237, China

Received: 7 August 2023

Accepted: 4 November 2023

Published online:
26 November 2023

© The Author(s), under
exclusive licence to Springer
Science+Business Media, LLC,
part of Springer Nature, 2023

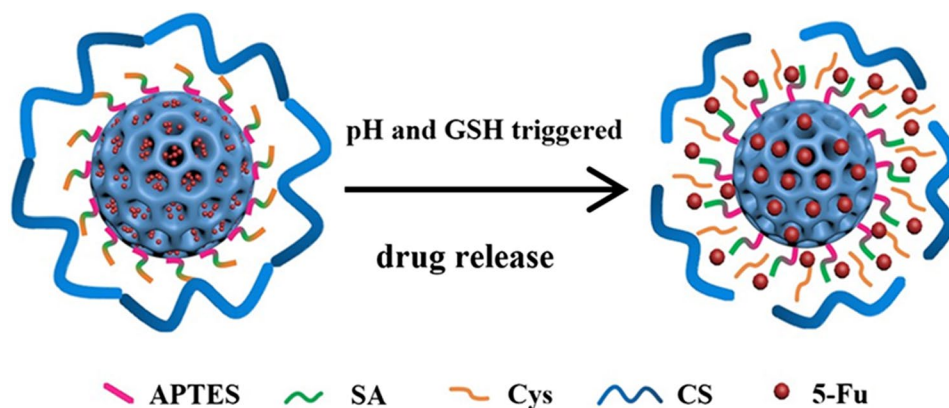
ABSTRACT

It is urgent to develop functional nanocarriers for targeted drug therapy of cancer. This work developed a smart drug controlled release system based on the dendritic mesoporous silica nanoparticle (DMSN) for dual gatekeepers drug delivery. The DMSN-Cys grafted with disulfide bonds appeared as spheres of uniform size with a porous structure, which enabled a drug loading efficiency of 68.32%. Since the protonated amino groups of chitosan were responsive to pH and the disulfide bonds were sensitive to glutathione, the modified 5-Fu@DMSN-Cys/CS can be used for pH/GSH responsive drug delivery. Release behaviors showed excellent drug controlled release effects. Good biocompatibility and pronounced cytotoxicity of 5-Fu@DMSN-Cys/CS were confirmed by cytotoxicity test. Noted specially, the microcosmic adsorption interaction between drug molecules and DMSN-Cys has been evaluated through molecular dynamic simulation. Electrostatic potential and adsorption simulation confirmed that the driving force of 5-Fu adsorption was originated from electrostatic force and hydrogen bonding interaction between the nanocarriers and 5-Fu molecules. These results indicated that 5-Fu@DMSN-Cys/CS could be potential carriers for anticancer drug delivery.

Handling Editor: Steven Naleway.

Address correspondence to E-mail: chenguie@sit.edu.cn; yjing05@sit.edu.cn; chemxuzl@ecust.edu.cn

GRAPHICAL ABSTRACT



Introduction

Globally, cancer has continuously become one of the fast-growing diseases and exploring effective therapeutic method with minimum side effects has become considerably significant [1, 3]. In spite of the advances in chemotherapy, cancer remains among the major causes of mortality [4, 5]. Therefore, it is urgent to develop effective drug delivery systems to treat cancer.

5-Fluorouracil (5-Fu) is an effective anticancer drug, which is extensively used to treat breast cancer, pancreatic cancer, liver as well as other cancers [6, 7]. 5-Fu has been widely used in clinical applications, but its application has been fully limited due to its drug resistance and rapid metabolism [8, 9]. Consequently, it is of great significance to develop more effective drug delivery systems for 5-Fu, controlling drug release into diseased tissues, and improving therapeutic efficiency [10, 11].

Due to the unique advantages of mesoporous silica nanoparticles (MSN) such as large specific surface area, high pore volume, well-defined pore structure, adjustable pore size, good biocompatibility as well as easily surface functionalization, it was considered a promising candidate drug for drug delivery as a drug carrier [12, 16]. Numpilai et al. investigated the effects of physicochemical properties of porous silica materials conjugated with dexamethasone via pH-responsive hydrazone bond on drug loading and release behavior [17]. But numerous studies showed that drug only adsorbed on the surface of drug carriers due to the small interaction force and

pore size, leading to the limited drug loading capacity and premature drug leakage [18, 20]. Notably, dendritic mesoporous silica nanoparticles (DMSN) with center-radial mesostructure have attracted increasingly attention in drug delivery process owing to their unique dendritic mesopore channels and high specific pore volume, enabling the encapsulation of large payloads [21, 25]. Lu et al. prepared badminton-like asymmetric modified mesoporous silica carriers by etching and following asymmetric modification [26]. As we all known that the pH value in tumor tissues is lower than that of normal tissue [27, 29], and the intracellular concentration of glutathione (GSH) is about 2–3 levels higher than that in extracellular plasma [30, 32]. These results have prompted us to design pH/GSH responsive nanocarriers for drug controlled release. Therefore, we hoped to develop dual stimuli-responsive nanocarriers based on DMSN to achieve the delivery of 5-Fu in tumor environments.

In this paper, we explored the modified DMSN to achieve the GSH and pH responsive drug delivery (Fig. 1). Sulfur-containing compounds were grafted onto the surface of DMSN through amide bonds, thereby introducing disulfide bonds. After that, chitosan as capping agents was applied to reduce drug leakage from the nanocarrier. The grafted Cys and the chitosan layer acted as ‘gate-keeper’ to control drug release in response to tumor cell microenvironment. Therefore, it can be imagined that functionalized DMSN with large specific surface area and pore volume could load more 5-Fu and realize stimuli-responsive drug release, which could enhance the

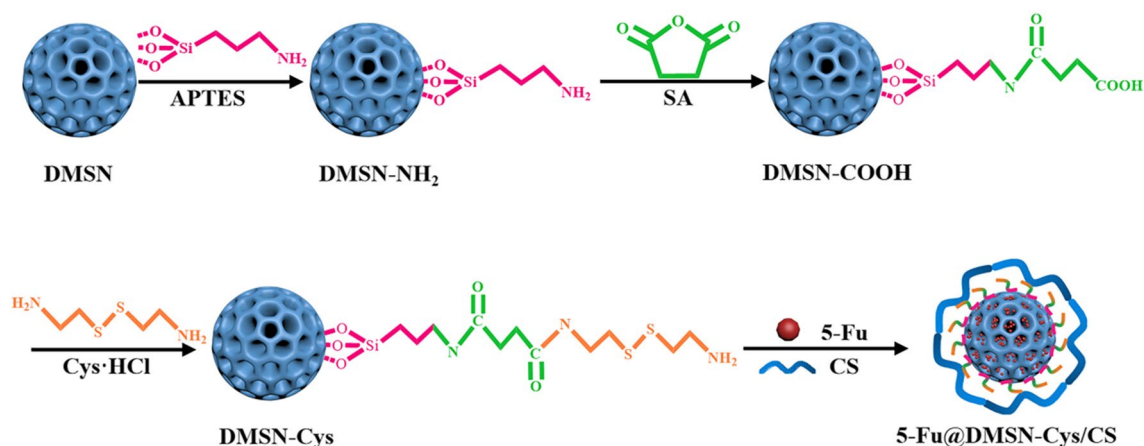


Figure 1 Schematic illustration of the fabrication of 5-Fu@DMSN-Cys/CS.

drug delivery efficiency. In vitro release study indicated that 5-Fu@DMSN-Cys/CS had control release performance and pH/GSH responsive capacity. The biocompatibility and cytotoxicity of 5-Fu@DMSN-Cys/CS were evaluated. Additionally, the adsorption simulation calculation showed that the interaction between 5-Fu and the grafted DMSN-Cys was stronger than the bare DMSN, which provided a theoretical basis for improving the loading capacity and sustained-release performance of microspheres on 5-Fu molecules.

Experimental

Materials

Tetraethyl orthosilicate (TEOS, 98%), hexadecyl trimethyl ammonium bromide (CTAB, >99%), (3-aminopropyl)triethoxysilane (APTES, 98%), triethanolamine (TEA), phosphate buffer solution (pH 7.4 and 5.0), sodium salicylate (NaSal, $\geq 99.5\%$), glutathione (GSH, 98%) and 5-fluorouracil (5-Fu, $\geq 98\%$) were bought from Shanghai Aladdin Biochemical Technology Co., Ltd. N-hydroxysuccinimide (NHS, 98%), succinic anhydride (SA, 99%), 1-(3-dimethylaminopropyl)-3-ethylcarbodiimide hydrochloride (EDC, 98%), cystamine dihydrochloride (Cys, >97%), dimethyl sulfoxide (DMSO) and chitosan (deacetylation degree 86%) were purchased from Shanghai Titan Scientific Co., Ltd. Cell Counting Kit-8 (CCK-8) was obtained from Shanghai Junzhe Biotechnology Co., Ltd.

Preparation of DMSN

Briefly, DMSN was prepared by modification of a one-pot method from the literature [33]. Typically, TEA (0.068 g) was dissolved in 50 mL water and stirred for 0.5 h at 80 °C. After that, CTAB (0.38 g) and NaSal (0.168 g) were dispersed into the reaction solution and stirred for another 1 h. Then, 2.0 mL of TEOS was added and continued to be stirred for 2 h. The nanoparticles were gathered via centrifuging and washed, sintered at 550 °C for 5 h.

Preparation of DMSN-COOH

0.5 g of DMSN was scattered in 50 mL anhydrous ethanol. After the addition of APTES (0.8 mL), the solution was refluxed at 80 °C for 20 h. The ammoniated nanoparticles were collected by centrifugation and drying. Next, SA (1.04 g) and TEA (0.7 mL) were added to DMSO containing 0.8 g of DMSN-NH₂ and stirred at 50 °C for 2 days to obtain DMSN-COOH.

Preparation of DMSN-Cys

0.5 g of DMSN-COOH was placed in 50 mL of DMSO solution in the presence of EDC (0.5 g) and NHS (0.5 g) with stirring for 2 h in room temperature. Cys (1.5 g) and TEA (0.67 mL) were then dissolved in the mixture upon stirring for another 24 h. Finally, the resulting solid was washed with ethanol and water, centrifuged and dried with lyophilization. DMSN-Cys nanoparticles were obtained.

Fabrication of 5-Fu@DMSN-Cys via encapsulation

0.1 g of DMSN-Cys was immersed into 45 mL pH 7.4 PBS, followed by adding 0.075 g of 5-Fu. The nanoparticles were collected by centrifugation and rinsed to remove the unloaded drug and named 5-Fu@DMSN-Cys. The loading amount of 5-Fu was measured by using a standard curve at the wavelength of 265 nm (Fig. S1). The loading capacity (LC) and encapsulation efficiency (EE) were investigated using the following equation:

$$LC(\%) = \frac{\text{weight of loaded 5-Fu}}{\text{weight of nanocarrier}} \times 100 \quad (1)$$

$$EE(\%) = \frac{\text{weight of loaded 5-Fu}}{\text{initial weight of 5-Fu}} \times 100 \quad (2)$$

Preparation of 5-Fu@DMSN-Cys/CS

To block the mesoporous channel, chitosan was used to coat the 5-Fu@DMSN-Cys. Briefly, 1.0 g of chitosan was added to 2% acetic acid aqueous solution and stirred for 12 h in room temperature. After obtaining transparent chitosan solution (1% w/v), 5-Fu@DMSN-Cys was supplemented to 40 mL of chitosan solution and mixed another 24 h. Finally, the 5-Fu@DMSN-Cys/CS was centrifuged and dried.

Drug release test in vitro

The in vitro release curve of 5-Fu@DMSN-Cys/CS was investigated the changes of 5-Fu under different pH and GSH concentrations. Typically, 5-Fu@DMSN-Cys/CS dispersed in 4 mL of PBS was placed in a dialysis bag, which embedded in 50 mL of the release solution and kept shaking at 37 °C. At the specified time, 2 mL of the release solution was sampled for analysis and fresh medium with equal volume was added. The release amount of 5-Fu was estimated by using UV-Vis spectrophotometer from its absorbance at 265 nm.

Cytotoxicity test

The biocompatibility of DMSN-Cys and the anticancer ability of 5-Fu@DMSN-Cys/CS were investigated by

cell counting kit-8 (CCK-8) method. MCF-7 and L929 cells were seeded in 96-well plate with a concentration of $8 \times 10^3 \text{ mL}^{-1}$ and were incubated with 100 μL nanoparticles dispersions containing two samples of different concentrations (12.5–200 $\mu\text{g mL}^{-1}$) for 24 h. Then, 120 μL CCK-8 was injected into these wells and incubated at 37 °C again for 2 h, and the relative cell viability was assessed by monitoring the absorbance at 450 nm.

Computational methods

This article used Materials Studio (MS) software to complete adsorption simulation, mainly including three modules: MS Visualizer, DMol³ and Forcite. MS visualizer: 5-Fu molecular, cluster and mixture model construction, model visualization and output; DMol³: geometric optimization and electrostatic potential analysis of 5-Fu molecule; forcite: geometric optimization of adsorption models, calculation and analysis of molecular dynamics. The relevant calculation parameter settings are shown in Table S1.

Characterization

The morphology of nanoparticles was affirmed by transmission electron microscopy (TEM, FEI Talos F200X) and scanning electron microscopy (SEM, Sigma 300). The particle size distribution and the zeta potential were determined through Malvern Zetasizer Nano ZS90. Nitrogen (N₂) adsorption-desorption isotherms was measured by using ASAP 2460. The pore volume and pore size distributions were obtained from the Barrett-Joyner-Halenda (BJH) method. The UV-Vis analysis was measured using a UV-2550 spectrophotometer. X-ray photoelectron spectrometer (XPS, ESCALAB 250Xi spectrometer) and Fourier transform infrared (FTIR) spectra (Nicolet 170SX spectrometer) were used to evaluate the composition of nanoparticles. Cytotoxicity was determined using a microplate reader (Tecan Spark 10 M).

Results and discussion

Morphology characterization of 5-Fu@DMSN-Cys/CS

From Fig. 2 a and b, DMSN had spherical, center-radial mesostructure and uniform open dendritic mesopore

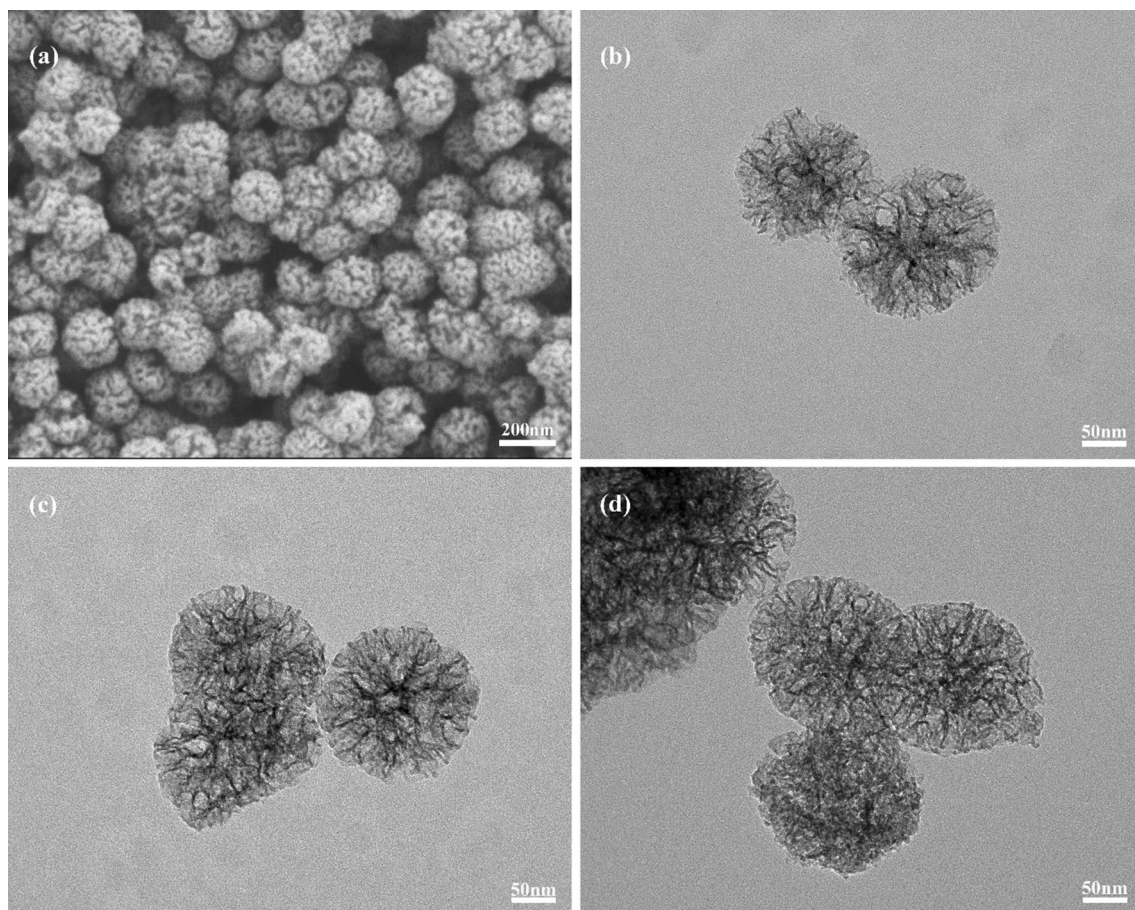


Figure 2 SEM image of **a** DMSN; TEM image of **b** DMSN, **c** DMSN-Cys, and **d** 5-Fu@DMSN-Cys/CS.

with the average particle size of 164 ± 14 nm. DMSN-Cys and 5-Fu@DMSN-Cys/CS have become slightly rough on the surface and blocked pores (Fig. 2 c, d). In addition, the mesopore arrays cannot be clearly observed after the introduction of the groups and drug, confirming adequate drug loading and surface successful grafting. DLS showed that the particle size distribution of DMSN was evaluated to be 278 ± 5 nm (PDI = 0.235), which was slightly larger than the particle size observed by TEM (Fig. 3 a). This result might be owing to a small amount of aggregated nanocomposites in the solution [35].

N₂ adsorption–desorption analysis

By the N₂ adsorption/desorption isotherm shown in Fig. 3 b, DMSN and DMSN-Cys represented a classical type IV isotherm accompanied with a hysteresis loop, which confirmed the existence of a mesoporous structure [36]. The specific surface area, pore volume,

and mean diameter of bare DMSN were $540.6 \text{ m}^2/\text{g}$, $1.65 \text{ cm}^3/\text{g}$ and 10.33 nm , respectively. Noted that the BET specific surface area and the pore volume of DMSN-Cys were decreased to $343.02 \text{ m}^2/\text{g}$ and $1.2 \text{ cm}^3/\text{g}$, implying the successful synthesis of composite nanomaterials and the provision of sufficient space for drug loading.

Analysis of zeta potentials

The surface property of DMSN before and after modification was detected by analysis of zeta potentials. Figure 3 c shows that zeta potential of the bare DMSN was about -12.3 mV . The zeta potential of DMSN-NH₂ was reversed to 7.9 mV owing to the amino-group on the surface of DMSN. After conjugated with succinic anhydride, the zeta potential reduced to -20.4 mV , because of the presence of negatively charged carboxyl groups of DMSN-COOH [37]. The acquired DMSN-Cys was positively charged, owing to the surface

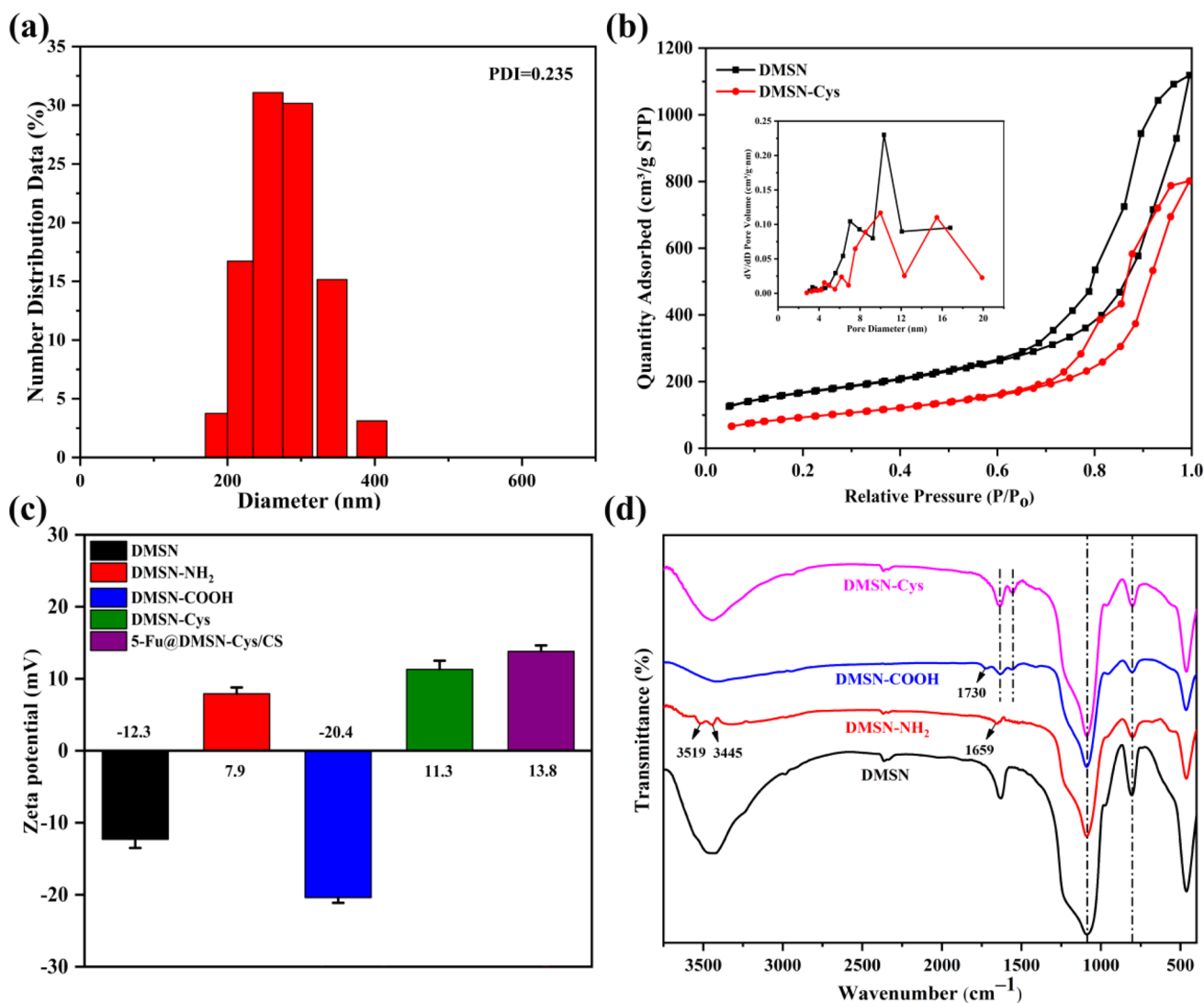


Figure 3 **a** Particle size distribution of DMSN; **b** N_2 adsorption/desorption isotherm and pore size distribution plot (inset) of DMSN and DMSN-Cys; **c** Zeta potentials of DMSN, DMSN-

NH₂, DMSN-COOH, DMSN-Cys and 5-Fu@DMSN-Cys/CS; **d** FT-IR spectra of DMSN, DMSN-NH₂, DMSN-COOH and DMSN-Cys.

residue of the amine group in the cysteamine. After coating of CS, the zeta potential of 5-Fu@DMSN-Cys/CS was further increased to 13.8 mV. The changes of zeta potential after every modification process have given evidence of successful functionalization.

FTIR analysis

The FTIR spectrum of DMSN, DMSN-NH₂, DMSN-COOH and DMSN-Cys is depicted in Fig. 3 d. The spectra of DMSN showed the absorption bands at 798 and 1091 cm^{-1} indicated the flexible vibration of Si-O

and the stretching vibration of Si-O-Si, respectively. For DMSN-NH₂, the presence of amine groups was evidenced by N-H stretching vibrations at 1659, 3445 and 3519 cm^{-1} . Moreover, three absorption bands were exhibited at 1730, 1635 and 1554 cm^{-1} , which were corresponded to C=O stretching vibration, stretching vibration of amide I and N-H stretching vibrations. The successfully functionalization with SA onto the surface of DMSN-NH₂ formed DMSN-COOH. Compared to DMSN-COOH, more stretching vibration peaks of amide I and N-H were introduced and the carboxyl group signal disappeared, suggesting coupling with cysteamine dihydrochloride [38].

All above results confirmed the successful functionalization of the nanocarrier.

XPS spectra of 5-Fu@DMSN-Cys/CS

The surface functionalization of 5-Fu@DMSN-Cys/CS was further confirmed by XPS analysis. The binding energy of O1s (532.5 eV), C1s (284.6 eV), Si2s (153.7 eV) and Si2p (103.3 eV) was detected in four samples (Fig. 4 a). In addition, new N1s and S2p peaks were observed in DMSN-NH₂ and DMSN-Cys, respectively, showing that amino and disulfide

bonds were successfully grafted onto the surface of DMSN. Compared with DMSN-Cys, there was new peak at 799 eV in the spectrum of 5-Fu@DMSN-Cys/CS, which was attributed to F1s. For the DMSN-Cys, the C1s peaks at 288.5, 285.6 and 284.6 eV were assigned to N–C=O, C–N and C–C bond (Fig. 4 b). Figure 4 c shows the N1s peaks at 399.9 and 400.6 eV which were bound with C–N and N–C=O bonds, respectively. The S2p peaks of DMSN-Cys at 163.5 and 164.6 eV were associated with C–S and –S–S– bond (Fig. 4 d), further demonstrating successful introduction of disulfide into DMSN-Cys [39].

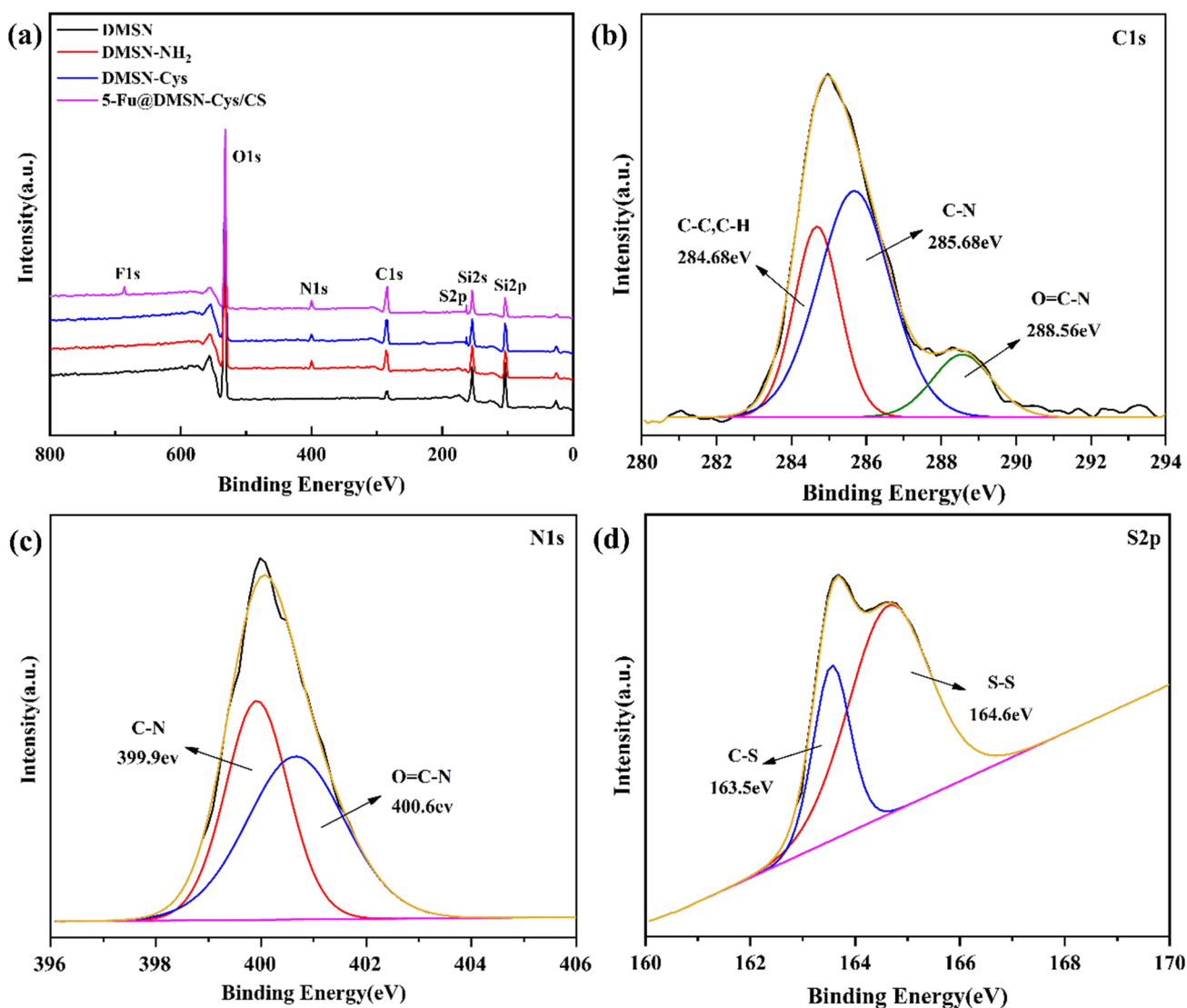


Figure 4 a XPS wide spectrum; b C1s, c N1s and d S2p spectra of DMSN-Cys nanoparticles.

Drug loading capacity

After the content of free 5-Fu was estimated by UV–Vis spectrophotometry at 265 nm, the loading capacity and encapsulation efficiency were 68.32% and 96.1%, respectively. Actually, compared to other nanocarriers used in previous studies, these efficiencies are very high [40, 41]. It is revealed that there are three reasons that explain the high DL of the prepared nanocomposites: (1) the pore structure, high specific surface area and the porosity of the nanoparticles, enhancing their ability to capture more drug molecules, (2) the presence of chitosan layer in the surface of nanocomposites prevented the diffusion of 5-Fu to the solution, and (3) the strong interactions between nanocomposite and 5-Fu, such as electrostatic interaction, van der Waals and hydrogen [42, 43].

In vitro release studies

In order to estimate the pH and GSH stimuli-responsive release characteristics, 5-Fu@DMSN-Cys/CS samples were immersed in different release medium (Fig. 5). There was no obvious burst drug release in the four drug release profiles. About 21.2% of 5-Fu was released at pH 7.4, whereas the amount release of 5-Fu reached to about 67.43% at pH 5.0, indicating that the rate of 5-Fu release from nanocarriers under physiological environments was slower than under acidic conditions. The sustained release of drugs was caused

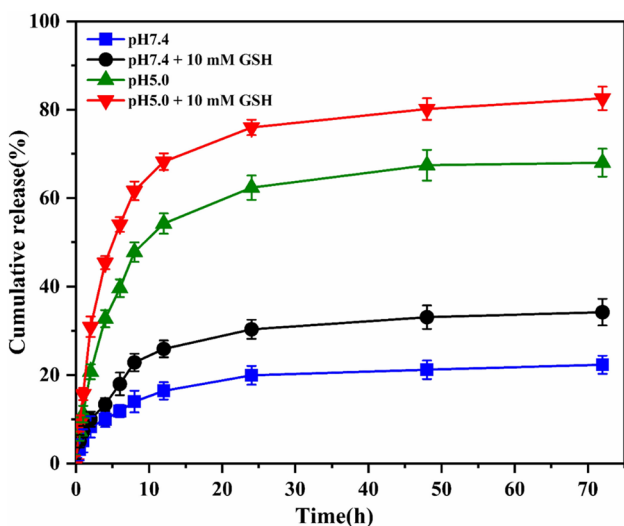


Figure 5 The 5-Fu release curve of 5-Fu@DMSN-Cys/CS under different GSH concentrations and different pH conditions.

by the cracking of the carrier matrix and the slow diffusion of drugs from the mesopores of nanocarriers. Nevertheless, the release of 5-Fu at pH of 7.4 was caused by drug adsorbed on the surface of the nanocarriers [44]. The high cumulative release rate under acidic conditions may be owing to the expansion of chitosan chains caused by the protonation amino groups of chitosan, which exposed the mesoporous channels of nanoparticles. However, chitosan chains acting as a shielding layer were coated on the surface of the modified nanoparticles to prevent drug leakage under neutral condition [45, 46]. Nearly 80.15% of 5-Fu was released at pH 5.0 + 10 mM GSH, which was 2.4-folds higher than that at pH 7.4 + 10 mM GSH. The result was caused by disulfide bonds (-S-S-) which were easily reduced to sulfhydryl groups (-SH) in high concentration GSH environments, leading to the collapse of cross-linked nanocarriers [47, 48]. Therefore, 5-Fu@DMSN-Cys/CS can achieve responsive transmission of GSH/pH, which is of great significance for cancer treatment.

In vitro cytotoxicity

The cytotoxicity of DMSN-Cys and 5-Fu@DMSN-Cys/CS was assessed by the CCK-8 method. As shown in Fig. 6 a, the drug-free carrier (DMSN-Cys) displayed little cytotoxicity against both L929 cells and MCF-7 cells, since the cell viability was more than 92% even at a high concentration of the drug-free carrier ($100 \mu\text{g mL}^{-1}$), implying excellent biocompatibility and non-toxic in vitro of the drug-free carrier. Noted that the 5-Fu@DMSN-Cys/CS exhibited concentration-dependent cytotoxicity against MCF-7 cells, with an increase in the toxicity directly proportional to the increase of the nanocarriers concentration. The cell viability of MCF-7 was only 62% when the concentration of the 5-Fu@DMSN-Cys/CS was $200 \mu\text{g mL}^{-1}$ (Fig. 6 b). In contrast, 89% of the L929 cells were still able to survive after being treated with the drug-loaded nanoparticles of the same concentration, demonstrating that the modified 5-Fu@DMSN-Cys/CS can effectively inhibit the growth of the MCF-7 cells without significant impact on normal cells.

Molecular dynamic simulation

Molecular dynamic simulation has been conducted for a better understanding of the adsorption interaction of 5-Fu with drug carriers (DMSN and DMSN-Cys).

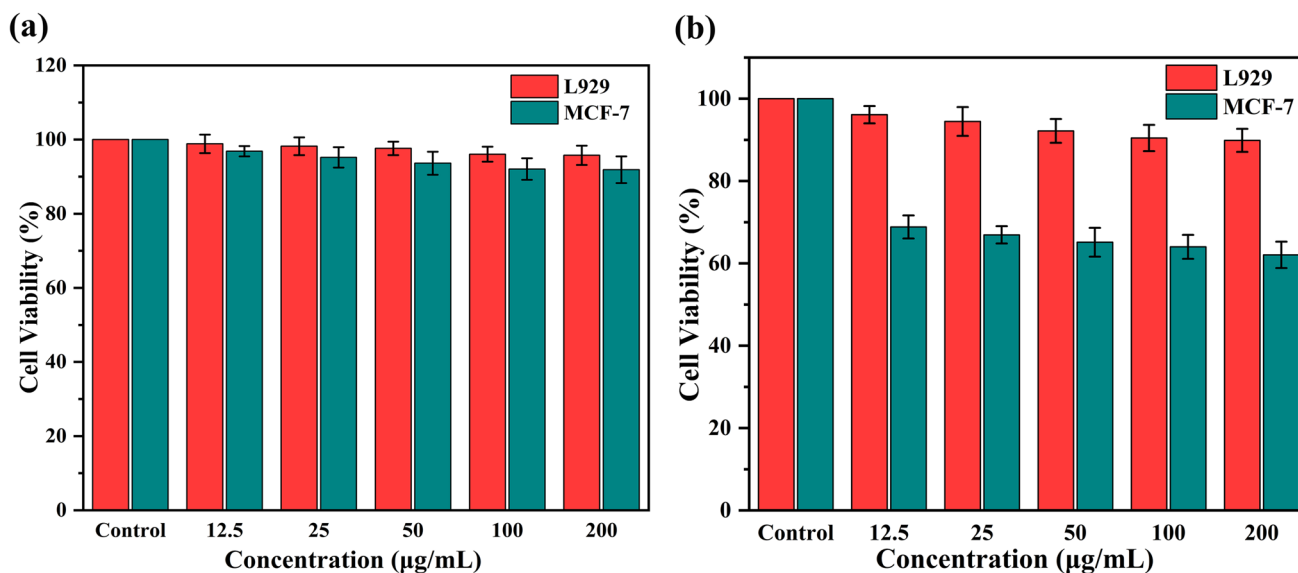


Figure 6 a Cytotoxicity of DMSN-Cys against L929 and MCF-7 cells; b Cytotoxicity of 5-Fu@DMSN-Cys/CS against L929 and MCF-7 cells.

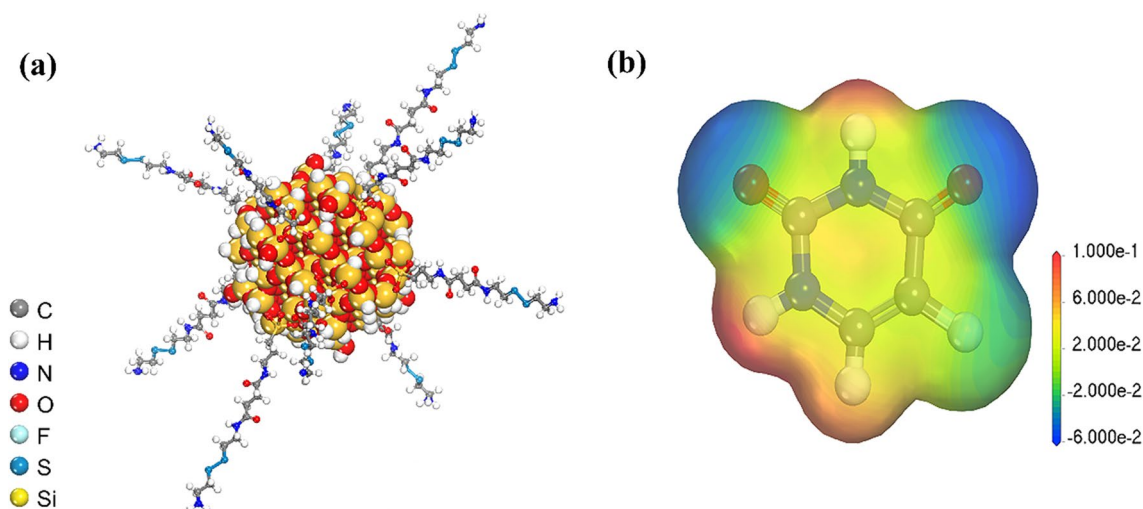


Figure 7 a The structure of DMSN-Cys; b molecular electrostatic potentials of 5-Fu.

The structures of the 5-Fu and DMSN are shown in Fig. S2. The structure of the DMSN-Cys is shown in Fig. 7 a, while the molecular electrostatic potentials of 5-Fu are given in Fig. 7 b. The blue region of 5-Fu molecule was negatively charged, which could adsorb positively charged atoms in DMSN or DMSN-Cys. On the contrary, the warm colored region was prone to adsorbing negatively charged atoms. The electrostatic interactions (attraction and repulsion) between atoms had an important impact on the adsorption process. Analyzing the electrostatic potential of 5-Fu

was of great significance for analyzing the interaction mechanism between drug and DMSN or DMSN-Cys. -F, -C=O and N in -NH of 5-Fu molecule exhibited significant negative charge, while H in -NH exhibited positive charge. The former was prone to adsorbing positively charged atoms such as hydroxyl hydrogen on DMSN or amino hydrogen and hydroxyl hydrogen on DMSN-Cys. The latter adsorbed with negatively charged atoms such as hydroxyl oxygen on DMSN, amino nitrogen and carbonyl oxygen on DMSN-Cys [49].

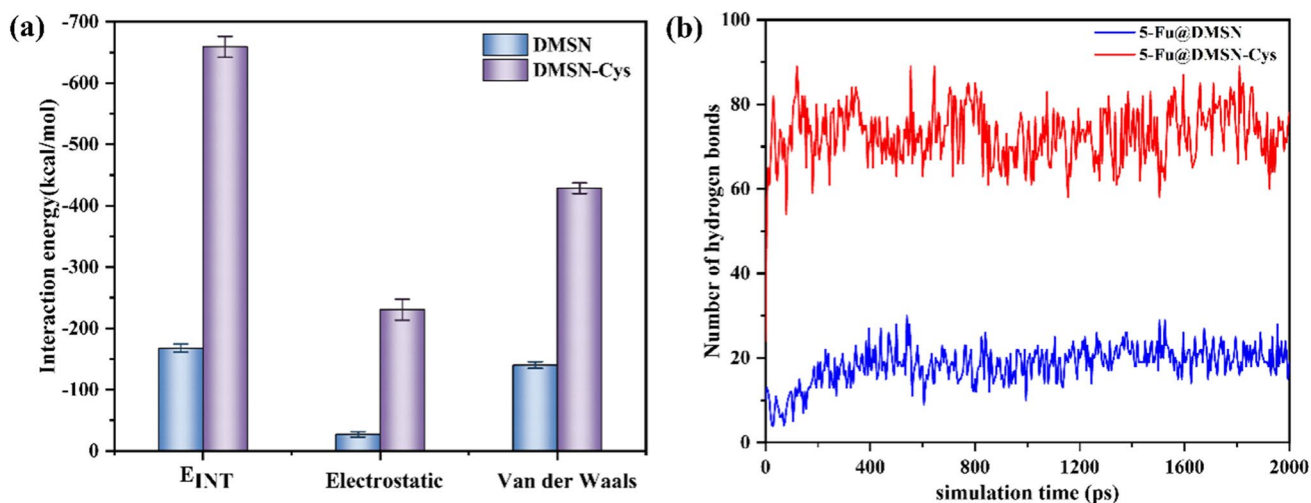


Figure 8 **a** The strength of the adsorption between 5-Fu molecules and DMSN or DMSN-Cys model; **b** curve of the number of hydrogen bonds in different adsorption models over simulation time.

Table 1 Number of hydrogen bonds between 5-Fu and different models

Model	Number of hydrogen bonds
5-Fu@DMSN	20.2 ± 3.1
5-Fu@DMSN-Cys	73.0 ± 6.2

The adsorption process of two adsorption models is shown in Fig. S3. As shown in Fig. 8 a, the binding energy (E_{int}) of both adsorption models was negative, indicating that there was adsorption between 5-Fu molecule and DMSN or DMSN-Cys. Absolute value of the E_{int} of 5-Fu@DMSN-Cys model was obviously greater than that of 5-Fu@DMSN model. In addition, the electrostatic force contribution of 5-Fu@DMSN model accounted for less than 17% of the E_{int} , while that of 5-Fu@DMSN-Cys model accounted for 35% of the E_{int} , indicating that the introduction of polar groups ($-NH_2$, $-NH$, $-C=O$) could significantly enhance the electrostatic force between 5-Fu and DMSN-Cys. Based on the molecular electrostatic potential analysis mentioned earlier, it can be seen that 5-Fu molecule with obvious positive and negative charged atoms will actively participate in the electrostatic adsorption process. The number of hydrogen bonds for 200 samples was counted the last 1000 ps of dynamic simulation. The results are shown in Fig. 8 b and Table 1. The number of hydrogen bonds in the 5-Fu@DMSN-Cys model was much more compared

with 5-Fu@DMSN model. There were more hydrogen bonds between DMSN-Cys and 5-Fu, due to the introduction of polar groups on DMSN made it easier to form hydrogen bonds. In a word, the electrostatic force between the modified nanocarrier and drug was stronger than that of the original particle. As shown in Fig. S4, 5-Fu@DMSN can cause sudden release of the drug in a short period of time, with an accumulation trend of increasing first and then decreasing, leading to large-scale loss and leakage of drugs. The relatively rapid release in the first four hour is due to the fact that the electrostatic interactions and hydrogen bond of naked DMSN on drugs were less than 5-Fu@DMSN-Cys/CS [49]. In addition, it was also possible that the drug loaded on the external surface of DMSN was first hydrolyzed and released, and then gradually leaked out of the mesopores, resulting in a decrease in drug accumulation [44]. Therefore, the adsorption simulation results evidenced that the modified nanocarrier had the advantages of sustained and controlled release, which was consistent with the results of release experiments.

Conclusions

In summary, a dual-sensitive nanocarrier based on uniform size of the modified DMSN as an anticancer delivery system was fabricated. The drug delivery system had high loading capacity and excellent pH/GSH responsiveness. After loading 5-Fu, the disulfide

bonds and CS were selected as gatekeeper to denote as 5-Fu@DMSN-Cys/CS. The drug releasing efficiency was up to 80.15% at pH 5.0 with 10 mM GSH, showing good tumor environment targeting performance. The results of cytotoxicity test reveal that the 5-Fu@DMSN-Cys/CS had good biocompatibility and pronounced cytotoxicity against MCF-7 cells. Molecular dynamic simulation indicated that the excellent sustained release performance of DMSN-Cys originated from interactions between DMSN-Cys and 5-Fu. These results concluded that the synthesized 5-Fu@DMSN-Cys/CS nanocarrier could be very promising new candidates for the application in drug delivery.

Acknowledgements

This work was supported by the National Natural Science Foundation of China (Nos. 22078092 and 21176067).

Author contributions

SNZ contributed to conceptualization, methodology and writing—original draft. RHT and SJD contributed to validation. GEC contributed to supervision and project administration. JY contributed to supervision and writing—review & editing. ZLX contributed to funding acquisition.

Funding

The funding was provided by National Natural Science Foundation of China, (22078092), Zhen-Liang Xu, (21176067), Zhen-Liang Xu

Data and code availability

Not applicable.

Declarations

Conflict of interest The authors declare that there is no conflict of interest in this paper.

Ethical approval None.

Supplementary Information The online version contains supplementary material available at <https://doi.org/10.1007/s10853-023-09128-5>.

References

- [1] Wang X, Yang L, Chen CZ (2008) Application of nanotechnology in cancer therapy and imaging. *CA Cancer J Clin* 58:97–110. <https://doi.org/10.3322/ca.2007.003>
- [2] Szekeres T, Novotny L (2002) New targets and drugs in cancer chemotherapy. *Med Princ Pract* 11:117–125. <https://doi.org/10.1159/000063243>
- [3] Bray F, Ferlay J, Soerjomataram I et al (2018) Global cancer statistics 2020: GLOBOCAN estimates of incidence and mortality worldwide for 36 cancers in 185 countries. *CA: Cancer J Clin*, 71:209–249
- [4] Fayyaz F, Yar M, Gulzar A, Ayub K (2022) First principles calculations of the adsorption of fluorouracil and nitrosourea on CTF-0; organic frameworks as drug delivery systems for cancer treatment. *J Mol Liq* 356:118941. <https://doi.org/10.1016/j.molliq.2022.118941>
- [5] Arruebo M, Vilaboa N, Saez-Gutierrez B et al (2011) Assessment of the evolution of cancer treatment therapies. *Cancers* 3:3279–3330. <https://doi.org/10.3390/cancers3033279>
- [6] Shakerzadeh E (2017) Quantum chemical assessment of the adsorption behavior of fluorouracil as an anticancer drug on the B36 nanosheet. *J Mol Liq* 240:682–693. <https://doi.org/10.1016/j.molliq.2017.05.12>
- [7] Dhinasekaran D, Raj R, Rajendran AR et al (2020) Chitosan mediated 5-Fluorouracil functionalized silica nanoparticle from rice husk for anticancer activity. *Int J Biol Macromol* 156:969–980. <https://doi.org/10.1016/j.ijbio mac.2020.04.098>
- [8] Choudhury H, Pandey M, Yin TH (2019) Rising horizon in circumventing multidrug resistance in chemotherapy with nanotechnology. *Mater Sci Eng C* 101:596–613. <https://doi.org/10.1016/j.msec.2019.04.00>
- [9] Jaferian S, Negahdari B, Eatemadi A (2016) Colon cancer targeting using conjugates biomaterial 5-fluorouracil. *Biomed Pharmacother* 84:780–788. <https://doi.org/10.1016/j.biopha.2016.10.004>
- [10] Dongsar TT, Dongsar TS, Gupta N et al (2023) Emerging potential of 5-Fluorouracil-loaded chitosan nanoparticles in cancer therapy. *J Drug Deliv Sci Technol* 82:104371. <https://doi.org/10.1016/j.jddst.2023.104371>
- [11] Anggraini SA, Prasetija KA, Yuliana M et al (2023) pH-responsive hollow core zeolitic-imidazolate framework-8 as an effective drug carrier of 5-fluorouracil. *Mater Today*

- Chem 27:101277. <https://doi.org/10.1016/j.mtchem.2022.101277>
- [12] Siddiqui B, Rehman AU, Haq IU, Al-Dossary AA et al (2022) Exploiting r-ecent trends for the synthesis and surface functionalization of mesoporous silica nanoparticles towards biomedical applications. *Int J Pharm X* 4:100116. <https://doi.org/10.1016/j.ijpx.2022.100116>
- [13] Peter J, Nechikkattu R, Mohan A et al (2021) Stimuli-responsive organic-inorganic mesoporous silica hybrids: a comprehensive review on synthesis and recent advances. *Mater Sci Eng B* 270:115232. <https://doi.org/10.1016/j.mseb.2021.115232>
- [14] Zhou M, Xing Y, Li W et al (2020) Thioether-bridged mesoporous organosilica nanocapsules with weak acid-triggered charge reversal for drug delivery. *Microporous Mesoporous Mater* 302:110242. <https://doi.org/10.1016/j.micromeso.2020.110242>
- [15] Numpilai T, Muenmee S, Witoon T (2016) Impact of pore characteristics of silica materials on loading capacity and release behavior of ibuprofen. *Mater Sci Eng C* 59:43–52. <https://doi.org/10.1016/j.msec.2015.09.095>
- [16] Hu Y, Dong X, Ke L et al (2017) Polysaccharides/mesoporous silica nanoparticles hybrid composite hydrogel beads for sustained drug delivery. *J Mater Sci* 52:3095–3109. <https://doi.org/10.1007/s10853016-0597-x>
- [17] Numpilai T, Witoon T, Chareonpanich M, Limtrakul J (2017) Impact of physicochemical properties of porous silica materials conjugated with dexamethasone via pH-responsive hydrazone bond on drug loading and release behavior. *Appl Surf Sci* 396:504–514. <https://doi.org/10.1016/j.apsusc.2016.10.183>
- [18] Maity A, Polshettiwar V (2017) Dendritic fibrous nanosilica for catalysis, energy harvesting, carbon dioxide mitigation, drug delivery, and sensing. *Chem Sus Chem* 10:3866–3913. <https://doi.org/10.1002/cssc.201701076>
- [19] Mei X, Chen D, Li N et al (2012) Hollow mesoporous silica nanoparticles conjugated with pH-sensitive amphiphilic diblock polymer for controlled drug rel-ease. *Microporous Mesoporous Mater* 152:16–24. <https://doi.org/10.1016/j.micromeso.2011.12.015>
- [20] Huang X, Tao Z, Praskavich JC et al (2014) Dendritic silica nanomaterials (KCC-1) with fibrous pore structure possess high DNA adsorption capacity and effectively deliver genes in vitro. *Langmuir* 30:10886–10898. <https://doi.org/10.1021/la501435a>
- [21] Malekmohammadi S, Mohammed RUR, Samadian H et al (2022) Nonorder-ed dendritic mesoporous silica nanoparticles as promising platforms for advanced methods of diagnosis and therapies. *Mater Today Chem* 26:101144. <https://doi.org/10.1016/j.mtchem.2022.101144>
- [22] Wan M, Zhao Y, Li H, Zou X, Sun L (2023) pH and NIR responsive polydopaminedoped dendritic silica carriers for pesticide delivery. *J Colloid Interface Sci* 632:19–34. <https://doi.org/10.1016/j.jcis.2022.11.009>
- [23] Zhang X, Zhao Y, Cao L, Sun L (2018) Fabrication of degradable lemon-like porous silica nanospheres for pH/redox-responsive drug release. *Sens Actuators B* 257:105–115. <https://doi.org/10.1016/j.snb.2017.10.104>
- [24] Du X, Shi B, Liang J et al (2013) Developing functionalized dendrimer-like silica nanoparticles with hierarchical pores as advanced delivery nanocarriers. *Adv Mater* 25:5981–5985. <https://doi.org/10.1002/adma.201302189>
- [25] Deng C, Liu Y, Zhou F et al (2021) Engineering of dendritic mesoporous silica nanoparticles for efficient delivery of water-insoluble paclitaxel in cancer therapy. *J Colloid Interface Sci* 593:424–433. <https://doi.org/10.1016/j.jcis.2021.02.098>
- [26] Lu J, Zhong W, Hou J, Zhao Y (2023) Fabrication of badminton-like porous silica carriers and their application in drug release. *Colloid Surf A* 670:131592. <https://doi.org/10.1016/j.colsurfa.2023.131592>
- [27] Zhu X, Wang CQ (2016) pH and redox-operated nanovalve for size-selective cargo delivery on hollow mesoporous silica spheres. *J Colloid Interface Sci* 480:39–48. <https://doi.org/10.1016/j.jcis.2016.06.043>
- [28] Yuan L, Tang Q, Yang D et al (2011) Preparation of pH-Responsive mesoporous silica nanoparticles and their application in controlled drug delivery. *J Phys Chem C* 115:9926–9932. <https://doi.org/10.1021/jp201053d>
- [29] Xiao D, Jia H-Z, Zhang J et al (2014) A dual-responsive mesoporous silica nanoparticle for tumor-triggered targeting drug delivery. *Small* 10:591–598. <https://doi.org/10.1002/sml.201301926>
- [30] Jiao J, Li X, Zhang S et al (2016) Redox and pH dual-responsive PEG and chitosan-conjugated hollow mesoporous silica for controlled drug release. *Mater Sci Eng C* 67:26–33. <https://doi.org/10.1016/j.msec.2016.04.091>
- [31] Du X, Kleitz F, Li X et al (2018) Disulfide-bridged organosilica frameworks: designed, synthesis, redox-triggered biodegradation, and nanobiomedical applications. *Adv Funct Mater* 28:1707325. <https://doi.org/10.1002/adfm.201707325>
- [32] Cheng R, Feng F, Meng F et al (2011) Glutathione-responsive nano-vehicles as a promising platform for targeted intracellular drug and gene delivery. *J Control Release* 152:2–12. <https://doi.org/10.1016/j.jconrel.2011.01.030>
- [33] Shen D, Yang J, Li X et al (2014) Biphasic stratification approach to three-dimensional dendritic biodegradable

- mesoporous silica nanospheres. *Nano Lett* 14:923–932. <https://doi.org/10.1021/nl404316v>
- [34] Yang Y, Bernardi S, Song H et al (2016) Anion assisted synthesis of large pore hollow dendritic mesoporous organosilica nanoparticles: understanding the composition gradient. *Chem Mater* 28:704–707. <https://doi.org/10.1021/acs.chemmater.5b03963>
- [35] Tian Z, Xu Y, Zhu Y (2017) Aldehyde-functionalized dendritic mesoporous silica nanoparticles as potential nanocarriers for pH-responsive protein drug delivery. *Mater Sci Eng C* 71:452–459. <https://doi.org/10.1016/j.msec.2016.10.039>
- [36] Shao D, Gao Q, Sheng Y et al (2022) Construction of a dual-responsive dual-drug delivery platform based on the hybrids of mesoporous silica, sodium hyaluronate, chitosan and oxidized sodium carboxymethyl cellulose. *Int J Biol Macromol* 202:37–45. <https://doi.org/10.1016/j.ijbiomac.2022.01.033>
- [37] Chen C, Yao W, Sun W et al (2019) A self-targeting and controllable drug delivery system constituting mesoporous silica nanoparticles fabricated with a multi-stimuli responsive chitosan-based thin film layer. *Int J Biol Macromol* 122:1090–1099. <https://doi.org/10.1016/j.ijbiomac.2018.09.058>
- [38] Chen C, Sun W, Wang X et al (2018) pH-responsive nanoreservoirs based on hyaluronic acid end-capped mesoporous silica nanoparticles for targeted drug delivery. *Int J Biol Macromol* 111:1106–1115. <https://doi.org/10.1016/j.ijbiomac.2018.01.093>
- [39] Rui Q, Gao J, Yin Z-Z et al (2023) A biodegradable pH and glutathione dual-triggered drug delivery system based on mesoporous silica, carboxymethyl chitosan and oxidized pullulan. *Int J Biol Macromol* 224:1294–1302. <https://doi.org/10.1016/j.ijbiomac.2022.10.215>
- [40] Mal A, Prabhuraj RS, Malhotra R et al (2022) pH-responsive sustained delivery of doxorubicin using aminated and PEGylated mesoporous silica nanoparticles leads to enhanced antitumor efficacy in pre-clinical orthotopic breast cancer model. *J Drug Deliv Sci Technol* 77:103800. <https://doi.org/10.1016/j.jddst.2022.103800>
- [41] Narayan R, Gadag S, Cheruku SP et al (2021) Chitosan-glucuronic acid conjugate coated mesoporous silica nanoparticles: a smart pH-responsive and receptor-targeted system for colorectal cancer therapy. *Carbohydr Polym* 261:117893. <https://doi.org/10.1016/j.carbpol.2021.117893>
- [42] Rajaei M, Rashedi H, Yazdian F et al (2023) Chitosan/agarose/graphene oxide nanohydrogel as drug delivery system of 5-fluorouracil in breast cancer therapy. *J Drug Deliv Sci Technol* 82:104307. <https://doi.org/10.1016/j.jddst.2023.104307>
- [43] Qin Y, Huang Y, Li M et al (2021) Novel photothermal-responsive sandwich-structured mesoporous silica nanoparticles: synthesis, characterization, and application for controlled drug delivery. *J Mater Sci* 56:12412–12422. <https://doi.org/10.1007/s10853-021-06097-5>
- [44] Kheiri K, Sohrabi N, Mohammadi R, Amini-Fazl MS (2022) Preparation and characterization of magnetic nanohydrogel based on chitosan for 5-fluorouracil drug delivery and kinetic study. *Int J Biol Macromol* 202:191–198. <https://doi.org/10.1016/j.ijbiomac.2022.01.028>
- [45] Webb BA, Chimenti M, Jacobson MP, Barber DL (2011) Dysregulated pH: a perfect storm for cancer progression. *Nat Rev Cancer* 11:671–677. <https://doi.org/10.1028/nrc3110>
- [46] Zhang K, Ding C, Liu X et al (2019) A redox and pH dual-triggered drug delivery platform based on chitosan grafted tubular mesoporous silica. *Ceram Int* 45:22603–22609. <https://doi.org/10.1016/j.ceramint.2019.07.292>
- [47] Cui Y, Dong H, Cai X et al (2012) Mesoporous silica nanoparticles capped with disulfide-linked PEG gatekeepers for glutathione-mediated controlled release. *ACS Appl Mater Interfaces* 4:3177–3183. <https://doi.org/10.1021/am3005225>
- [48] Lee MH, Yang Z, Lim CW et al (2013) Disulfide-cleavage-triggered chemosensors and their biological applications. *Chem Rev* 113:5071–5109. <https://doi.org/10.1021/cr300358b>
- [49] Abdel-Bary AS, Tolan DA, Nassar MY et al (2020) Chitosan, magnetite, silicon dioxide, and graphene oxide nanocomposites: synthesis, characterization, efficiency as cisplatin drug delivery, and DFT calculations. *Int J Biol Macromol* 154:621–633. <https://doi.org/10.1016/j.ijbiomac.2020.03.106>

Publisher's Note Springer Nature remains neutral with regard to jurisdictional claims in published maps and institutional affiliations.

Springer Nature or its licensor (e.g. a society or other partner) holds exclusive rights to this article under a publishing agreement with the author(s) or other rightsholder(s); author self-archiving of the accepted manuscript version of this article is solely governed by the terms of such publishing agreement and applicable law.